International Journal of Refractory Metals and Hard Materials 141 (2026) 108007

Contents lists available at ScienceDirect

International Journal of Refractory Metals and Hard Materials

journal homepage: www.elsevier.com/locate/IJRMHM

Effect of the binder phase composition and volume fraction on the sintering behavior of extra-coarse WC-based hardmetals

Irene Salto Talaya [a,b,c], Lucía Muñoz-Ortuño [a,b], José M. Sánchez-Moreno [a,b], Unai Galech [a,b], Federico Ibarreta-López [d], Roberto Martínez-Pampliega [d], Adrián Durán Benito [c,e], Tomás Soria-Biurrun [a,b,*]

[a] CEIT-Basque Research and Technology Alliance (BRTA), Paseo de Manuel Lardizábal 15, 20018 Donostia/San Sebastián, Spain
[b] Universidad de Navarra, Tecnun, Paseo de Manuel Lardizábal 13, 20018 Donostia/San Sebastián, Spain
[c] BIOMA Institute, University of Navarra, 31008 Pamplona, Spain
[d] FMD CARBIDE, Fabricación Metales Duros, S.A.L., Gudarien Etorbidea 18, 48970 Basauri, Spain
[e] Department of Chemistry, School of Sciences, University of Navarra, 31008 Pamplona, Spain

ARTICLE INFO

Keywords:
Extra-coarse WC carbides
Alternative binders
Sinter-HIP
WC grain growth

ABSTRACT

This work investigates the sintering behavior and microstructural evolution of extra-coarse WC hardmetals using conventional Co and FeNiCo (40/40/20) (wt%) binder phases. Four compositions containing 15 and 20 wt% metallic binder were produced by powder metallurgy and consolidated by sinter-HIP at 1475 °C. Dilatometry and DSC analyses showed that replacing Co with FeNiCo significantly reduces sinterability, shifting densification to higher temperatures despite similar calculated liquid-phase fractions. This behavior is attributed to the lower solubility of WC in FeNiCo liquids compared with liquid Co. Microstructural characterization revealed complete densification and the elimination of W_2C after sintering. WC grain growth was strongly affected by binder chemistry. FeNiCo-bonded alloys exhibited more pronounced changes in grain size distribution with increasing binder content and developed more rounded WC morphologies than WC–Co grades. Hardness measurements confirmed a significant softening associated with FeNiCo substitution, mainly due to the intrinsically lower hardness of Ni-rich metallic matrices.

1. Introduction

Hardmetals with extra-coarse microstructures, i.e. with average WC grain sizes exceeding 6 μm, are particularly suitable for mining applications in which components are subjected to severe abrasion, impact loading and fatigue [1–9]. Typical wear mechanisms described in the literature include loss of binder phase, microfracture of WC grains and removal of the resulting WC fragments when binder retention is lost [2–4,7]. The performance of extra-coarse hardmetals is governed not only by the binder mean free path but also by the intrinsic mechanical properties of the metallic phase. Key parameters for controlling these properties are the WC grain size distribution after sintering and the volume fraction and chemical composition of the metallic binder, which critically depend on processing conditions. Promising results have been reported by mixing submicron and coarse WC powders, where WC grain growth is promoted because the submicron WC particles are dissolved in the liquid phase during sintering and subsequently precipitated on the surface of coarse WC grains [10–12]. With respect to binder phase chemistry, several metallurgical strategies have been explored to enhance hardness and strength, including precipitation hardening and high-entropy alloying concepts [13–16]. In parallel, as cobalt is classified as a critical raw material [17], increasing efforts are being directed toward its partial or complete replacement in WC-based cemented carbides for different applications [18–22]. Among these investigations, only limited information is available regarding the application of alternative binders in extra-coarse WC-based cemented carbides [23]. Existing studies have demonstrated that WC–FeNiCo extra-coarse cemented carbides can be consolidated to full density using conventional powder metallurgy routes while achieving reductions in cobalt content of up to 50%. However, detailed investigations addressing

* Corresponding author at: CEIT-Basque Research and Technology Alliance (BRTA), Paseo de Manuel Lardizábal 15, 20018 Donostia/San Sebastián, Spain.
E-mail addresses: isaltot@ceit.es (I.S. Talaya), lmunozortun@ceit.es (L. Muñoz-Ortuño), jsanchezm@ceit.es (J.M. Sánchez-Moreno), ugalech@ceit.es (U. Galech), fede.ibarreta@fmd-hm.com (F. Ibarreta-López), roberto.martinez@fmd-hm.com (R. Martínez-Pampliega), adrianduran@unav.es (A.D. Benito), tsoria@ceit.es (T. Soria-Biurrun).

https://doi.org/10.1016/j.ijrmhm.2026.108007
Received 8 June 2026; Received in revised form 10 July 2026; Accepted 17 July 2026
Available online 19 July 2026

dimensional control during sintering and the kinetics of WC grain growth remain lacking. For further reduction of the cobalt content in WC-based cemented carbides, the 40Fe–40Ni–20Co alloy (wt%) is being considered as one of the most promising candidates because it combines excellent sinterability, relatively wide carbon windows, and considerable flexibility for tailoring hardness, strength, and toughness [19,21]. In this context, the present work investigates the suitability of the 40Fe–40Ni–20Co alloy as a binder phase for the sintering of hardmetals produced from WC powders with an average particle size exceeding 10 μm.

2. Experimental procedure

The extra-coarse (EC) WC powder grade selected for this study, supplied by Wolfram Bergbau und Hütten AG, exhibited an average particle size of 15.7 μm (Fig. 1 and Table 1). Scanning electron microscopy (SEM) observations revealed the presence of well-defined grain boundaries on the surface of most particles, thereby confirming their polycrystalline nature (Fig. 2). To investigate the internal structure of these coarse WC aggregates, the powders were embedded in a Cu matrix. This was achieved by mixing EC-WC powders with pure Cu powders and subsequently melting the mixture at 1200 °C in a graphite crucible placed inside a muffle furnace under flowing H_2 atmosphere. A heating rate of 20 °C/min was employed without any holding stage at the maximum temperature. Under these conditions, neither WC dissolution nor significant grain growth was detected. Polished cross-sections of the embedded WC particles revealed that carburization was not fully completed in some of the extra-coarse particles (Fig. 3). Backscattered electron SEM (BSE-SEM) micrographs showed the presence of bright cores within the coarser particles, indicating, according to *Z*-contrast conditions, regions with higher W/C ratios than those corresponding to the outer portions of the particles. X-ray diffraction (XRD) with Ni-filtered CuKα radiation and Bragg-Brentano configuration was also used to confirm the presence of W_2C, in agreement with SEM observations. Although the intensity of the corresponding diffraction peaks was low, it remained above the detection limit of the equipment (approximately 1 vol%) (Fig. 4). Carbon analyses performed by infrared combustion indicated over-stoichiometric carbon contents in the EC-WC powders (Table 1), suggesting the presence of free carbon. This excess carbon was likely either intentionally added for carbon control during sintering or remained unreacted after the production of the EC-WC powders. Oxygen contents were comparatively low, which is consistent with the low specific surface area characteristic of these coarse powders. The metallic powders selected for the binder phase consisted of Co powders supplied by Nanjing Hanrui Cobalt Co., Ltd., together with Fe and Ni carbonyl powders provided by Umicore (Fig. 5). The Fe carbonyl powders exhibited a characteristic spherical morphology and a relatively narrow particle size distribution (Table 1). SEM observations

Table 1
Characteristics of starting powders.

	Particle size distribution*			Chemical analysis (wt%)	
Ref.	D10	D50	D90	Carbon	Oxygen
EC_WC	8.9	15.7	28.3	6.14 ± 0.7	0.031 ± 0.001
Fe	3.0	5.7 (5.3)**	11.7	0.055 ± 0.001	0.74 ± 0.10
Ni	3.0	16.0 (1.1)**	50.1	0.19 ± 0.01	0.20 ± 0.01
Co	1.5	4.3 (1.7)**	11.0	0.06 ± 0.01	0.51 ± 0.02

* Measured by Dynamic Image Analysis (QICPIC/L & RODOS/L, M5).
** Average particle size (FSSS) provided by the suppliers.

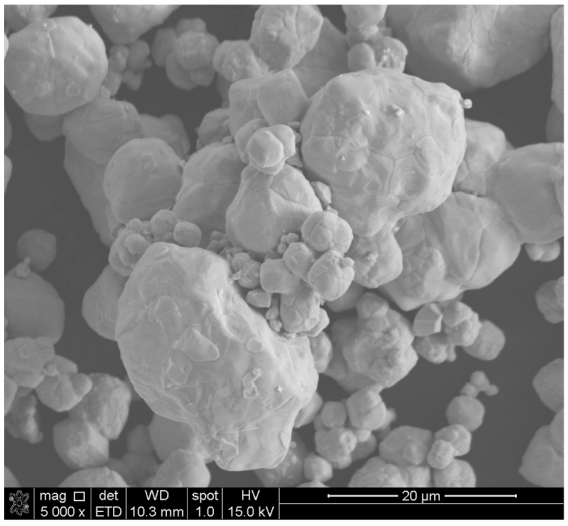

Fig. 2. SE-SEM image of extra-coarse WC powders (characteristics included in Table 1).

also showed that the Co and Ni powders were considerably finer, in agreement with the Fisher Sub-Sieve Sizer (FSSS) data provided by the manufacturers (Table 1). The larger particle sizes obtained by dynamic image analysis are attributed to the high degree of agglomeration exhibited by both Co and Ni powders, particularly the latter.

As summarized in Table 2, four hardmetal compositions were prepared using the powders described above. Alloys 1 and 2 contained Co as the sole binder constituent, with metallic binder contents of 15 and 20 wt%, respectively. Alloys 3 and 4 also contained 15 and 20 wt% metallic additions; however, in these materials, Co was replaced by a 40 wt%

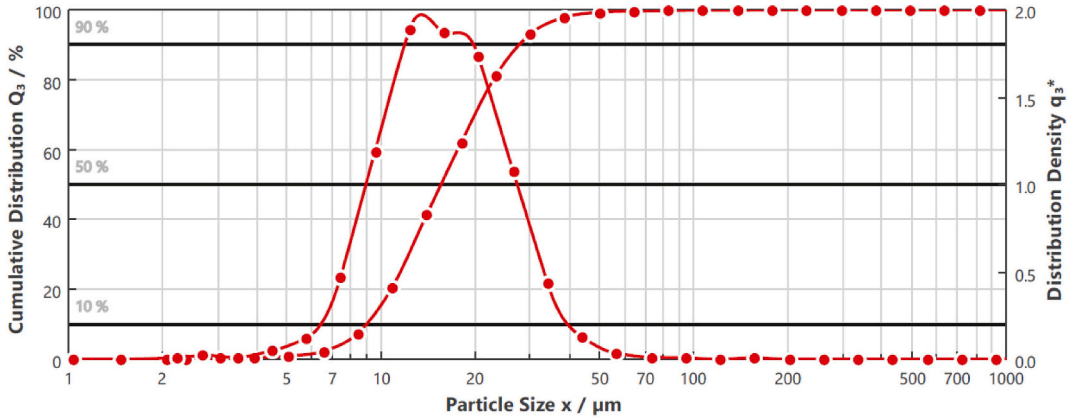

Fig. 1. Particle size distribution obtained by dynamic image analysis corresponding to extra-coarse WC powders in as-received condition.

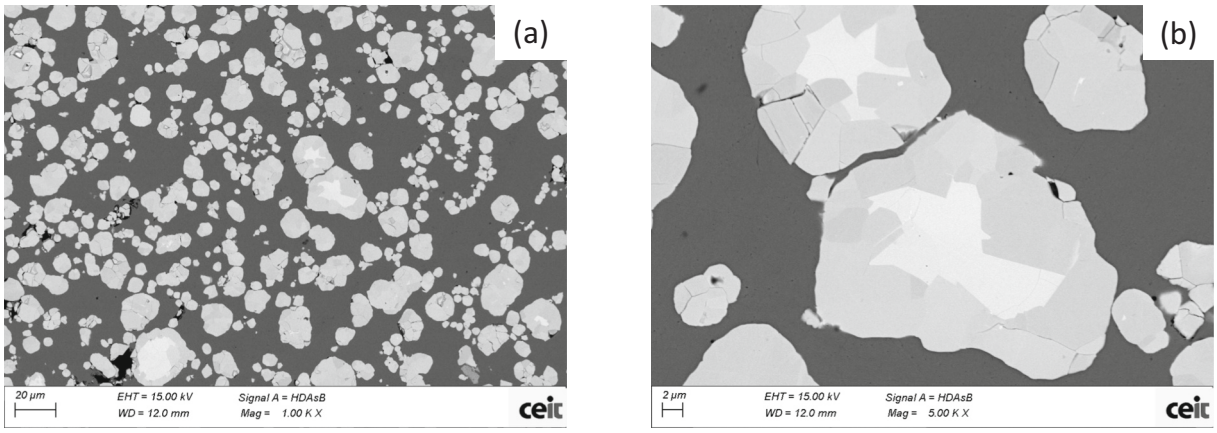

Fig. 3. BSE-SEM images of polished cross-sections of extra-coarse WC powder samples embedded in copper. Cores of coarser particles show brighter *Z*-contrast compatible with higher W/C ratios.

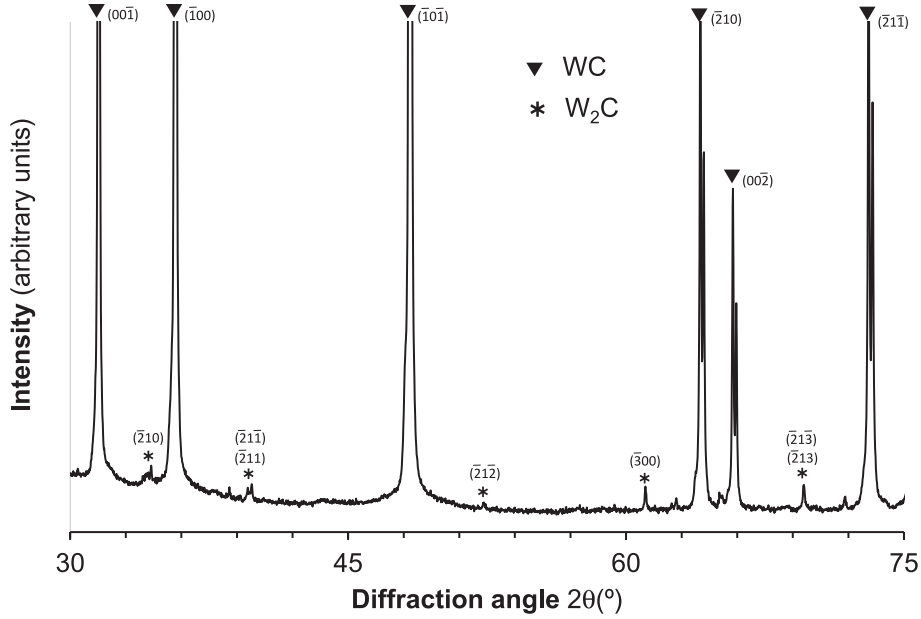

Fig. 4. XRD pattern of extra-coarse WC powders: ▼ WC ICDD-2025 PDF: 2102283 * W_2C ICDD-2025 PDF:1539792.

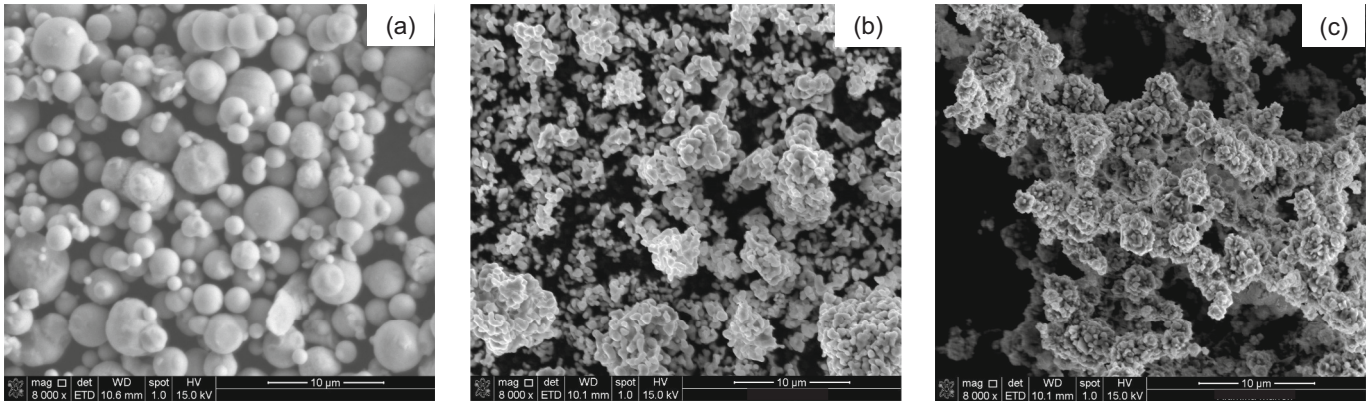

Fig. 5. SE-SEM images corresponding to the metallic powders used in the mixtures: (a) Fe carbonyl, (b) Ni carbonyl, (c) Co.

Fe–40 wt%Ni–20 wt%Co alloy, hereafter referred to as "FeNiCo". Powder mixing and milling were carried out in a planetary mill operating at 50 rpm for 5 h using ethanol as the milling medium and a ball-to-powder weight ratio of 6:1 (balls made of WC-6wt%Co material). Paraffin wax, used as a pressing aid, was added during the final hour of milling. Subsequently, the powder mixtures were dried for 40 min at

Table 2
Compositions of the powder mixtures (in wt%).

Alloy	EC-WC	Co	Fe	Ni
Alloy 1 (A1)	85	15	–	–
Alloy 2 (A2)	80	20	–	–
Alloy 3 (A3)	85	3	6	6
Alloy 4 (A4)	80	4	8	8

atmospheric pressure in a thermostatically controlled bath maintained at 80 ± 2 °C. Green compacts were produced by uniaxial pressing at 160 MPa. Paraffin removal was performed at 680 °C in a refractory muffle furnace under a H_2/N_2 protective atmosphere using a heating rate of 5 °C/min.

Following powder processing, differential scanning calorimetry (DSC), dilatometry, and vacuum sintering experiments were carried out. DSC analyses were performed using a TGA/DSC Setaram Setsys Evolution 16/18 system in order to determine the onset and endset temperatures associated with liquid-phase formation for each composition. Samples weighing 100 ± 20 mg were heated to 1400 °C at a rate of 10 °C/min and held for 10 min under flowing Ar atmosphere at 1 bar. Heating and cooling cycles were repeated twice to ensure complete homogenization of the binder constituents. Consequently, the onset and endset temperatures obtained during the second heating cycle were considered representative of the solidus and liquidus temperatures of each alloy. Dilatometric analyses were conducted under conditions identical to those used in the DSC experiments employing a Netzsch TA 402 E/7 dilatometer. Cylindrical specimens with both diameter and height equal to 6 mm were used. Final densification was performed in a sinter-HIP furnace equipped with graphite insulation and heating elements. Three pressure stages were applied during the thermal cycle: (i) 10^{-2} mbar during heating from room temperature to 1300 °C to promote degassing and carbothermal reduction of surface oxides; (ii) 100 mbar from 1300 °C up to 1475 °C and during the first 45 min of the holding stage to control binder evaporation; and (iii) 40 bar during the final 15 min at 1475 °C to eliminate residual porosity. Carbon contents in the sintered specimens were measured by infrared combustion analysis using a LECO CS-200 analyzer. Determination of the corresponding carbon windows additionally required detailed microstructural characterization by field-emission gun scanning electron microscopy (FEG-SEM). Prior to observation, specimens were ground and polished down to 1 μm diamond finish. WC grain sizes were determined using ImageJ software (National Institutes of Health, Bethesda, MD, USA) from backscattered electron images, which provided enhanced contrast between WC grains and the metallic binder. Grain size was evaluated as the equivalent circle diameter. For each composition, at least 600 WC grains were measured, resulting in an estimated relative error of approximately ±5%. Thermodynamic analyses of the experimental results were performed using Thermo-Calc software in combination with the TCFE13 commercial database for steels and a thermodynamic database developed in previous studies [20,22]. Finally, Vickers hardness was determined with 30 kg of applied load at room temperature (ISO 3878).

3. Results and discussion

3.1. Densification

Dilatometric curves corresponding to the extra coarse WC- metal alloys show that the substitution of Co by FeNiCo induces a significant loss of sinterability (Fig. 6a). Using the original height of the compacts as a reference (represented by the dotted blue line), it is confirmed that absolute shrinkage ($\Delta L < 0$) occurs at temperatures much higher for the compositions based on FeNiCo than on Co binders: at a temperature 263 °C higher for the alloys with 15 wt% of metallic addition (Alloys 1 and 3) and at 533 °C for those with 20 wt% of metal (Alloys 2 and 4).

A magnified view of the dilatometric curve during the heating ramp up to 1250 °C reveals that, although all alloys exhibit swelling, several relative solid-state contraction events occur between 500 °C and 700 °C (Fig. 6b). This change in trend may be associated with the carbothermal reduction of the oxides present in the samples, namely CoO, FeO, NiO, and WO_3, which would facilitate diffusion processes within the metallic phase leading to partial densification [21]. This is very effective in the case of Alloy 2, where one third of the volume (not considering porosity) is already thermally activated for spreading on the surface of WC particles and through prior WC-WC grain boundaries present in the powder (see Fig. 3). As observed in Fig. 6b, this leads to 2.5% linear shrinkage at 1200 °C, that is, 136 °C below the melting onset measured by DSC for this alloy (Table 3). In the other three compositions (Alloys 1, 3 and 4), swelling is more pronounced, especially above 800 °C in the materials with FeNiCo binder. Apart from thermal expansion itself, this swelling could be related to the porosity induced by interdiffusion of Fe, Co and Ni atoms in the new lattice generated during the alloying process (Kirkendall porosity) [24].

Densification in solid state is very limited in the four investigated alloys below 1300 °C, that is, very near the melting onset in all cases (Fig. 7). This is expected from the very low specific surface area of WC extra-coarse powders, which is the main driving force for solid state sintering in these materials [25]. As observed in the shrinkage rate vs. temperature plots, shrinkage is strongly accelerated in all compositions by the formation of the liquid phase.

As the wetting behavior of Fe, Co and Ni liquids on the surface of WC grains is reported to be very similar (i.e. in the three cases wetting angles

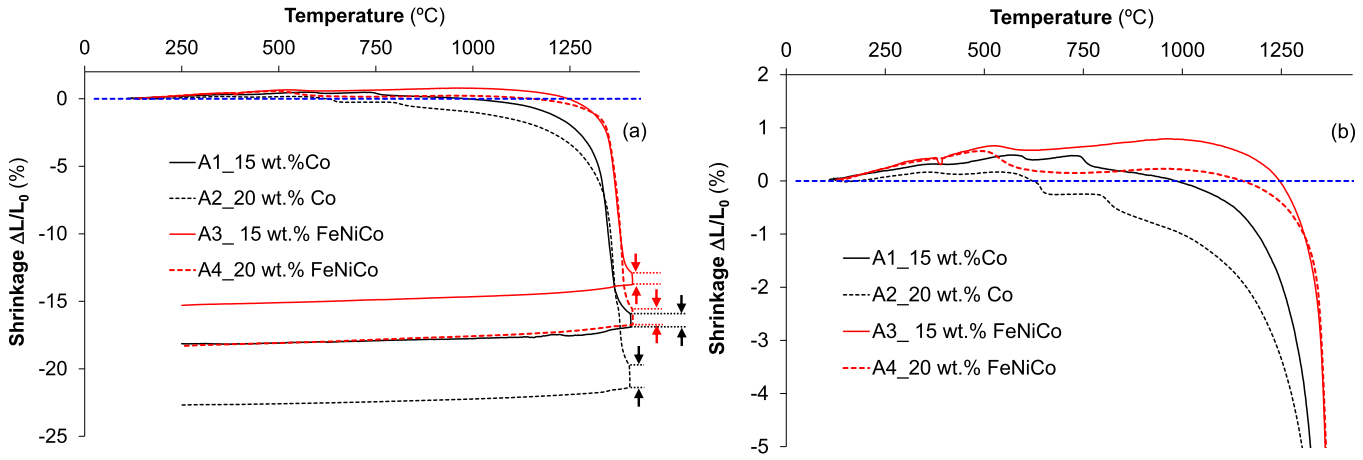

Fig. 6. (a) Shrinkage of extra-coarse WC-Co and WC-FeNiCo hardmetals with 15 and 20 wt% metallic addition, (b) zoom showing the initial swelling of the specimens during the heating ramp.

Table 3
Correlation between shrinkage rate and DSC peaks corresponding to the formation of the liquid phase during the heating ramp.

Ref.	Temperature (°C)					
	Dilatometry			DSC		
	Onset	Peak	Endset	Onset	Peak	Endset
Alloy 1 15 wt.% Co	1309	1342	1369	1337	1364	1370
Alloy 2 20 wt.% Co	1330	1354 1374	1389	1336	1364	1372
Alloy 3 15 wt.% FeNiCo	1334	1365	1394	1350	1378	1382
Alloy 4 20 wt.% FeNiCo	1330	1377	1395	1356	1385	1391

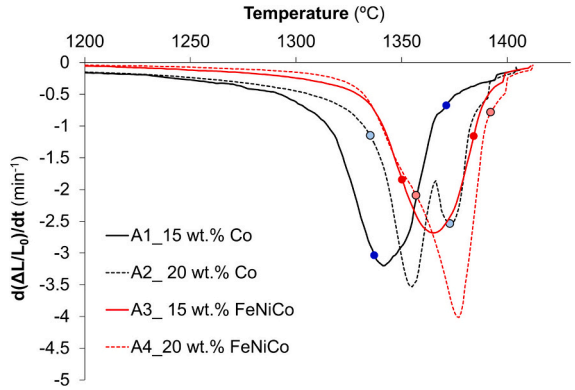

Fig. 7. Shrinkage rate curves corresponding to WC-Co and WC-FeNiCo hardmetals with 15 and 20 wt% metallic addition. Circles of the same color superimposed on each graph correspond to the beginning and end of melting during the heating ramp.

at 1500 °C are close to zero [26,27]), densification associated with rearrangement of WC grains due to capillary forces should be similar. However, liquid Co dissolves a much higher quantity of WC than Ni or Fe at the corresponding eutectic temperatures: 22 wt%, 12 wt% and 7 wt% respectively [28].

The importance of WC solubility in the liquid phase is evidenced by analyzing the effect of increasing the amount of metallic addition on shrinkage during the sintering plateau of 1 h at 1400 °C (marked by red and black arrows in Fig. 6a). During this isothermal dwelling, shrinkage is 71% higher when the amount of Co increases from 15 wt% to 20 wt% (Alloys 1 and 2, respectively). However, in EC_WC-FeNiCo materials (A3 and A4 alloys), the same increase in the metallic content leads to an increase in shrinkage of only 33% (Fig. 8). This is relevant considering that the calculated amount of liquid phase at 1400 °C in the four compositions is very similar for Co and FeNiCo alloys with the same metal addition: 31.5 vol% for Alloys 1 and 3 and 40.1 vol% for Alloys 2 and 4 (Fig. 9). These calculations are consistent with experimental measurements of the binder volume fraction after sintering (Table 4), suggesting that the solubility of WC grains in the liquid phase plays a key role in densification kinetics.

Both simulation-based and experimental data show that, for alloys based on Co binders, the onset, peak and endset temperatures are lower than FeNiCo binder alloys (Fig. 10 and Table 3). The C windows calculated with both the TCFE13_TC® database and the W-C-Fe-Ni-Co-Cr database generated in previous works [20,22] show that the sintered EC-WC-Co grades (A1 and A2) are closer to the boundary with the C-free region, and EC-WC-FeNiCo materials (A3 and A4) are closer to the "eta" phase precipitation boundary.

It is well known that, within the C-window, a reduction in carbon content leads to an increase in the temperature at which liquid-phase formation occurs [29]. This behavior is consistently captured by both the DSC results and the thermodynamic calculations. It is worth noting that, in WC-FeNiCo materials, both solidus and liquidus temperatures and the prediction of the roofing effect is better predicted with the database described in refs. [20, 22] than with the TCFE13® steel database. The model also predicts the shifting of the melting range toward higher temperatures when the binder volume fraction increases (Table 5).

3.2. Microstructural characterization of sinter-HIPed samples

SEM micrographs of the materials obtained after sinter-HIP at 1475 °C confirm the absence of both residual porosity and binder-phase pooling (Fig. 11). WC polycrystalline aggregates present in as-received extra-coarse WC powders (Figs. 2 and 3) are disintegrated by the combined action of different mechanisms, including fracturing induced during mixing with metallic powders, liquid penetration through WC-WC grain boundaries, etc. As expected, no W_2C is detected after sintering since the total C content has been adjusted to compensate the incomplete carburization of the powder (Table 1). Analysis of the grain size distributions obtained by ImageJ software (Fig. 12) shows that increasing the liquid-phase volume fraction produces a much larger relative increase in WC grain size in FeNiCo-based alloys than in Co-based alloys. This is because, owing to the much higher solubility of WC in the latter [19,21,29,30], the liquid formed with 15 wt% Co does not become saturated in W and C at the sintering temperature. Increasing the cobalt content to 20 wt% shifts the grain size distribution slightly toward larger sizes, with a significant effect only in the 8–10 μm fraction. In the remaining size fractions, the change is much smaller. In contrast, for the FeNiCo-based materials, the liquid becomes saturated

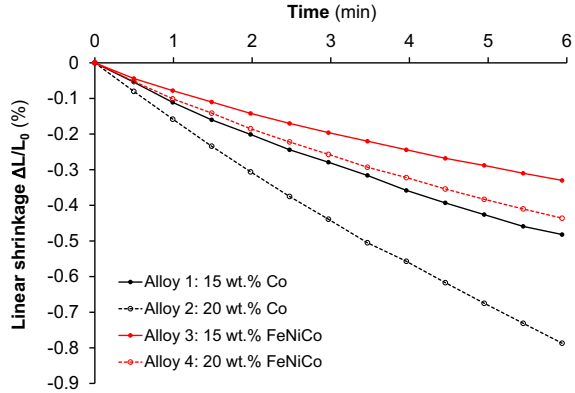

Fig. 8. Isothermal shrinkage vs. time (at 1475 °C) for WC-Co and WC-FeNiCo hardmetals with 15 and 20 wt% metallic addition.

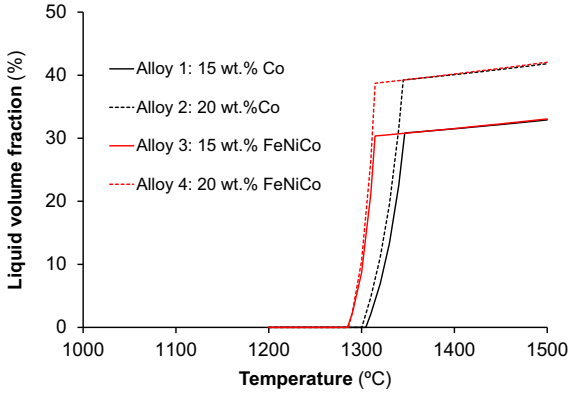

Fig. 9. Liquid volume fraction as a function of temperature calculated with Thermocalc® software and TCFE13 dabase.

Table 4
Metallic binder phase volume fraction (%) measured by Image J software on SEM images obtained from specimens sintered at 1475 °C for 1 h.

Ref.	WC area (μm^2)	Metal area (μm^2)	WC volume (%)	Metal volume (%)
Alloy 1	39027	12660	76	24
Alloy 2	35842	15844	69	31
Alloy 3	38444	13243	74	26
Alloy 4	35962	15724	70	30

when its volume fraction is low. Increasing it by approximately 33% (from A3 to A4) substantially enhances the diffusion of W and C, leading to significant changes across all WC grain size fractions (Fig. 12a).

It is also worth noting that the percentage of WC grains below 2 μm is double for Alloy 3 than for the rest of the materials (20% vs. 10%, respectively) (Fig. 12a). This finding is again consistent with the lower solubility of WC in the FeNiCo-based liquid when compared with that in liquid Co and has an effect of the WC-D50 value (Fig. 13).

As described by several authors, 2-D nucleation is the main WC coarsening mechanism during liquid phase sintering of hardmetals, leading to different morphologies depending on the carbon content of the system: from low truncation and elongation factors for high carbon activities to the opposite for low carbon ones [31–34]. In these experiments, the main morphological difference appears when substituting Co by FeNiCo (Fig. 14). These images show that WC grains in the WC-FeNiCo materials exhibit a more rounded morphology than those in the WC-Co alloys, where the grains are generally compatible with the truncated trigonal prism morphology. WC-Co hardmetals with rounded WC carbides have been produced starting with already rounded large WC powder particles and the correct addition of grain growth inhibitors (VC, Cr_3C_2) [35]. In our experiments, no grain growth inhibitors were added, therefore, the observed shape change is likely related to the different dissolution–reprecipitation behavior promoted by the FeNiCo binder. The lower solubility of WC in FeNiCo liquids is expected to reduce the extent of dissolution and subsequent reprecipitation during sintering, which may limit the development of well-defined crystallographic facets and result in a less faceted, more rounded grain morphology. Further TEM studies are currently underway to clarify the nature of the WC/binder interfaces.

The results of hardness tests carried out on extra-coarse hardmetals confirm the trends already reported for finer WC grades [19,21], namely that there is a significant softening associated with the substitution of Co by the FeNiCo (40/40/20) binder phase (Table 6): 18.6% for 15 wt% addition of binder and 23.1 wt% for 20 wt% binder content. As it is well known, nickel is significantly softer than cobalt because of its higher stacking fault energy. These results indicate that this effect is dominant in the FeNiCo austenitic binder phase, where solid-solution strengthening is insufficient to maintain the hardness levels achieved with cobalt-based matrices. However, this reduction cannot be attributed exclusively to the binder chemistry. Hardness is also affected by the binder content [29,36–38]. As shown in Table 6, increasing the binder content from 15 to 20 wt% decreases the hardness from 909 to 809 HV30 (Alloys 1 and 2) in the Co-bonded system and from 740 to 622 HV30 (Alloys 3 and 4) in the FeNiCo-bonded system. In addition, the WC median grain size (D50) increases from 4.2 to 4.5 μm (Alloys 1 and 2) and from 3.3 to 4.3 μm (Alloys 3 and 4). The increase in WC grain size is also expected to contribute to the reduction in hardness, as larger WC grains generally result in lower hardness values [29,36–38]. Therefore, the measured hardness reflects the combined effects of binder chemistry, binder content, and WC grain size.

4. Conclusions

This study evaluated the feasibility of using a 40Fe–40Ni–20Co (wt

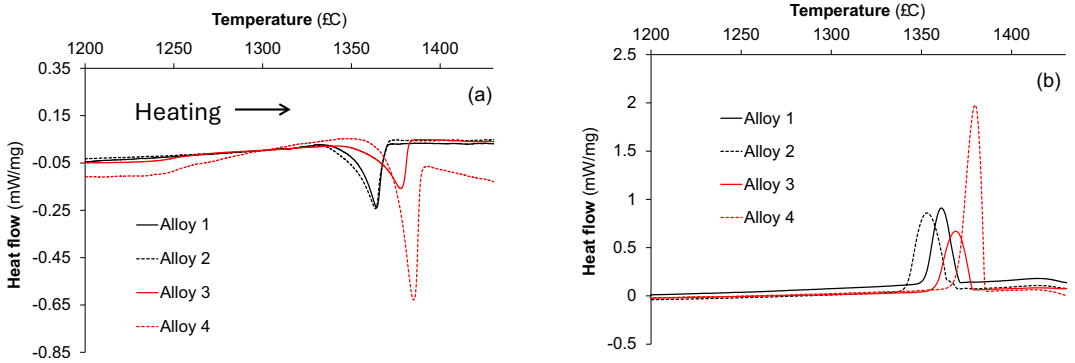

Fig. 10. DSC plots of the WC-Co and WC-FeNiCo hardmetals with 15 and 20 wt% metallic addition: (a) heating ramp, (b) cooling ramp.

Table 5
Temperatures corresponding to the beginning and end of melting of the liquid phase of alloys. C contents measured in specimens are also included. These data are compared to Thermocalc ® estimates (TCFE13 database and database developed in previous works [20,22]).

Ref.	Temperature (°C)					C content after sintering (wt.%)	Calculated C-window (wt%)
	ThermoCalc		DSC				
	Onset	Endset	Onset	Peak	Endset		
Alloy 1	1304*	1347*	1350	1364	1370	5.22 ± 0,01	5.02–5.23*
	1304**	1347**					5.03–5.24**
Alloy 2	1301*	1344*	1336	1364	1372	4.93 ± 0,02	4.65–4.94*
	1301**	1344**					4.65–4.94**
Alloy 3	1283*	1315*	1365	1378	1382	5.21 ± 0,02	5.15–5.28*
	1311**	1406**					5.17–5.29**
Alloy 4	1284*	1315*	1360	1385	1391	4.90 ± 0,02	4.82–5.00*
	1310**	1407**					4.85–5.00**

* TCFE13.
** Database developed in previous works [20,22].

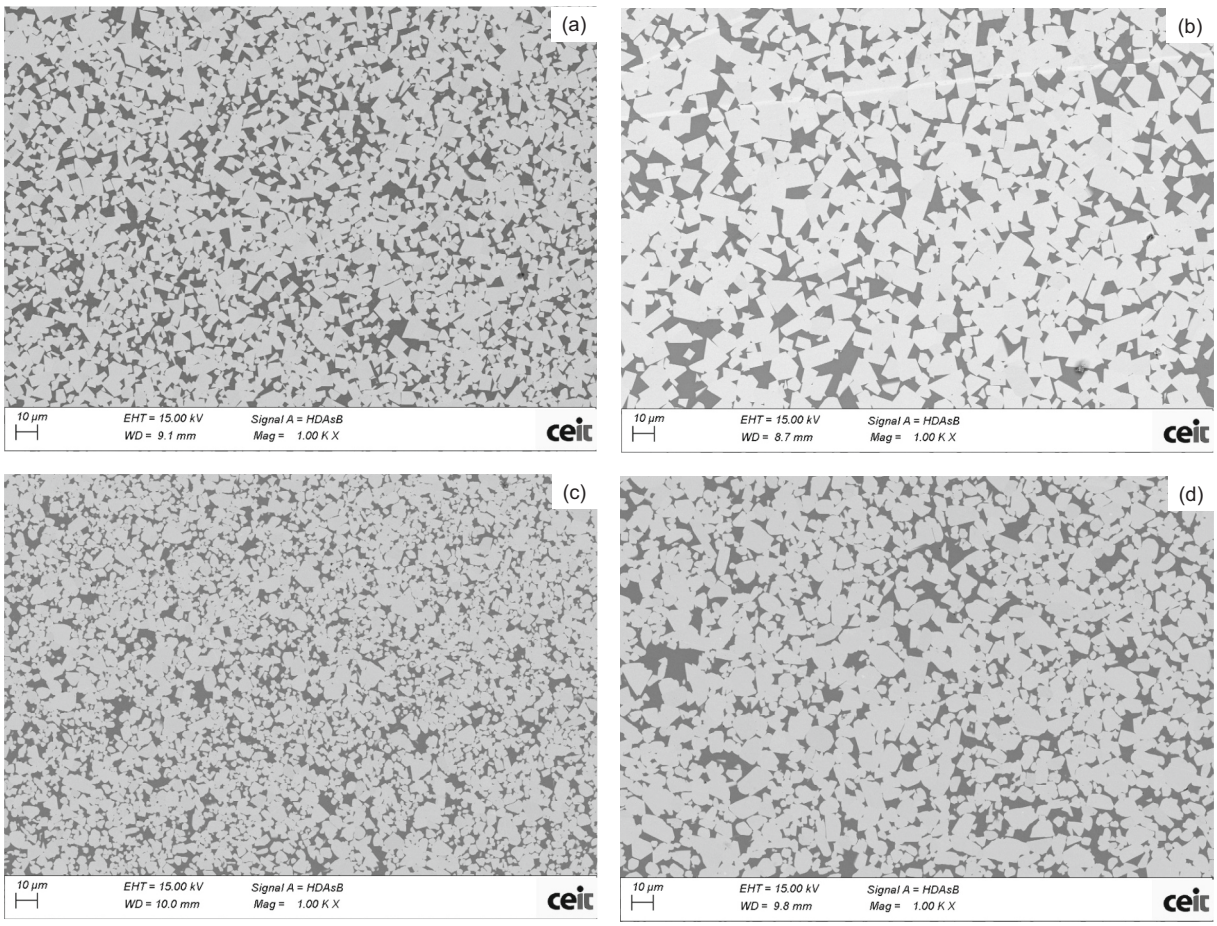

Fig. 11. HDAsB SEM micrographs corresponding to specimens sinter-HIPed at 1475 °C-40 bars- 1 h: (a) WC-15 wt%Co, (b) WC-20 wt%Co, (c) WC-15 wt% FeNiCo, (d) WC-20 wt%FeNiCo.

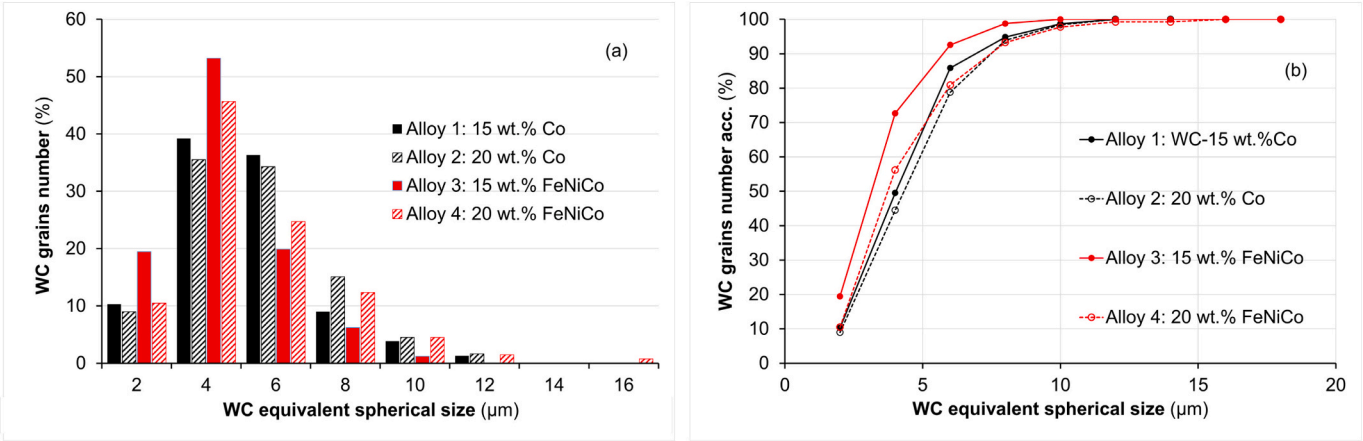

Fig. 12. WC grain size distributions in WC-Co and WC-FeNiCo hardmetals: (a) frequency plot, (b) cumulative plot.

%) alloy as an alternative binder phase in extra-coarse WC hardmetals and compared its behavior with that of conventional Co-bonded grades. Main conclusions are:

- The substitution of Co by FeNiCo significantly reduces the sinterability of extra-coarse WC hardmetals, shifting the onset of liquid-assisted densification to higher temperatures. This effect is observed despite similar calculated liquid-phase fractions in both systems.
- FeNiCo-based alloys exhibit higher solidus and liquidus temperatures than their Co-based counterparts, as confirmed by DSC measurements and thermodynamic modelling.
- Densification kinetics are strongly influenced by WC solubility in the liquid phase. The lower solubility of WC in FeNiCo liquids leads to reduced dissolution–reprecipitation activity and consequently slower shrinkage during liquid-phase sintering.
- All investigated compositions achieved full densification after sinter-HIP, and no residual W_2C was detected, indicating effective carbon

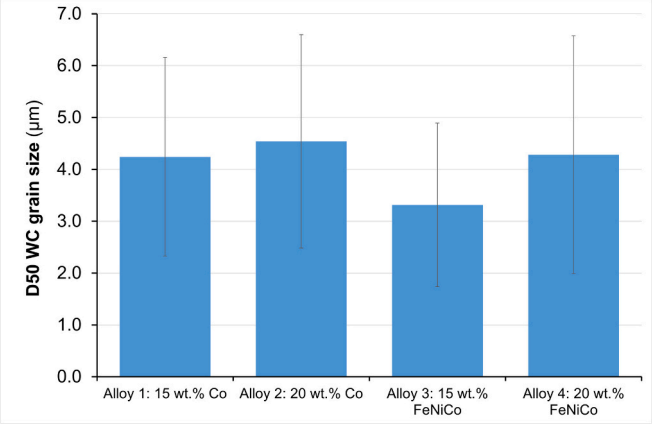

Fig. 13. WC D50 values corresponding to the WC grain size distributions of Fig. 12.

control and complete reaction with extra C additions during processing.

- WC grain growth is more sensitive to binder content in FeNiCo-based systems than in Co-based alloys. Increasing the metallic fraction produces a more pronounced shift in grain size distribution in FeNiCo-containing hardmetals.
- WC grains in FeNiCo-bonded materials display more rounded morphologies compared with the faceted truncated trigonal prism shapes typically observed in WC–Co systems, suggesting a modified balance between dissolution and reprecipitation processes.
- The observed softening in FeNiCo-based hardmetals is mainly attributed to the intrinsically lower hardness of FeNiCo austenite, which cannot fully compensate through solid-solution strengthening effects.

Overall, FeNiCo alloys represent a viable but mechanically softer alternative to Co binders, offering distinct sintering and microstructural evolution characteristics that must be carefully considered for extra-coarse WC hardmetal design.

CRediT authorship contribution statement

Irene Salto Talaya: Writing – original draft, Investigation, Data curation. **Lucía Muñoz-Ortuño:** Writing – review & editing. **José M. Sánchez-Moreno:** Writing – review & editing, Validation, Supervision, Resources, Methodology, Investigation, Funding acquisition, Formal analysis, Data curation, Conceptualization. **Unai Galech:** Writing – review & editing. **Federico Ibarreta-López:** Writing – review & editing.

Table 6
Vickers hardness HV30 vs. WC D50 grain size for WC-Co and WC-FeNiCo extra-coarse cemented carbides.

Ref.	WC grain size D50 (µm)	Hardness HV30 (kg/mm^2)
Alloy 1 (15 wt%Co)	4.2 ± 1.9	909 ± 18
Alloy 2 (20 wt.% Co)	4.5 ± 2.1	809 ± 15
Alloy 3 (15 wt.% FeNiCo)	3.3 ± 1.6	740 ± 17
Alloy 4 (20 wt.% FeNiCo)	4.3 ± 2.3	622 ± 14

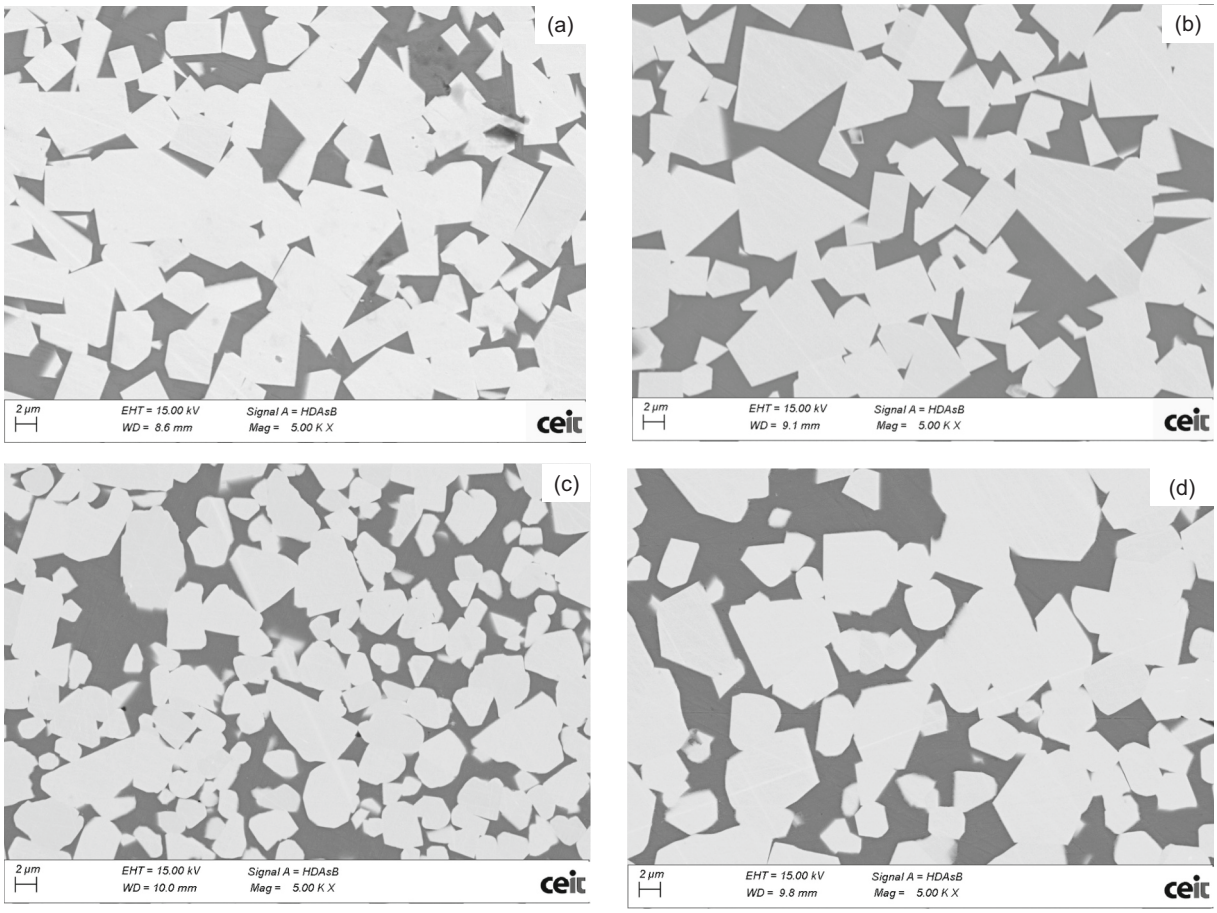

Fig. 14. High-magnification HDAsB SEM micrographs illustrating the differences in WC grain morphology: (a) WC–15 wt% Co, (b) WC–20 wt% Co, (c) WC–15 wt% FeNiCo, and (d) WC–20 wt% FeNiCo.

Roberto Martínez-Pampliega: Writing – review & editing. **Adrián Durán Benito:** Writing – review & editing, Supervision. **Tomás Soria-Biurrun:** Writing – review & editing, Writing – original draft, Validation, Supervision, Software, Methodology, Investigation, Funding acquisition, Formal analysis, Data curation, Conceptualization.

Declaration of competing interest

The authors declare that they have no known competing financial interests or personal relationships that could have appeared to influence the work reported in this paper.

Acknowledgments

Irene Salto Talaya thanks the BIOMA Institute for her doctoral grant.

Data availability

All the data and results supporting this research paper are already provided within this publication.

References

[1] I. Konyashin, B. Ries, Wear damage of cemented carbides with different combinations of WC mean grain size and Co content, part II: laboratory performance tests on rock cutting and drilling, Int. J. Refract. Met. Hard Mater. 23 (2005) 225–232.
[2] U. Beste, S. Jacobson, A new view of the deterioration and wear of WC/Co cemented carbides rock rill buttons, Wear 264 (2008) 1129–1141.
[3] J. Angseryd, A. From, J. Wallin, S. Jacobson, S. Norgren, On a wear test for rock drill inserts, Wear 301 (2013) 109–115.
[4] X. Yang, S. Wu, Y. Kang, X. Wang, R. Xia, Pitting mechanism of cemented carbide tool in the early stage of rock drilling, Int. J. Refract. Met. Hard Mater. 42 (2014) 103–107.
[5] P.K. Katiyar, P.K. Singh, R. Singh, A.l. Kumar, Modes of failure of cemented tungsten carbide tool bits (WC/Co): a study of wear parts, Int. J. Refract. Met. Hard Mater. 54 (2016) 27–38.
[6] S. Momeni, S. Moseley, M. Ante, J. Allaart, The wear of WC-Co bits during rotary-percussive drilling of reinforced concrete, Int. J. Refract. Met. Hard Mater. 62 (B) (2017) 202–209.
[7] H. Jones, S. Norgren, M. Kritikos, K. Mingard, M. Gee, Examination of wear damage to rock-mining hardmetal drill bits, Int. J. Refract. Met. Hard Mater. 66 (2017) 1–10.
[8] J. Heinrichs, S. Norgren, S. Jacobson, M. Olsson, Influence of cemented carbide binder type on wear initiation in rock drilling investigated in sliding wear against magnetite rock, Int. J. Refract. Met. Hard Mater. 85 (2019) 105035.
[9] S. Moseley, S. Momeni, Wear phenomena in different cemented carbides during rotary-percussive drilling in reinforced concrete, Int. J. Refract. Met. Hard Mater. 108 (2022) 105941.
[10] R. He, B. Li, P. Ou, C. Yang, H. Yang, J. Ruan, Effects of ultrafine WC on the densification behavior and microstructural evolution of coarse-grained WC-5Co cemented carbides, Ceram. Int. 46 (2020) 12852–12860.
[11] Z. Lu, J. Du, Y. Sun, G. Su, C. Zhang, X. Kong, Effect of ultrafine WC contents on the microstructures, mechanical properties and wear resistances of regenerated coarse grained WC-10Co cemented carbides, Int. J. Refract. Met. Hard Mater. 97 (2021) 105516.
[12] H. Wang, Y. Liu, J. Ye, Effects of nano WC and Cr_3C_2 on grain growth, microstructure and mechanical properties of ultra-coarse cemented carbides, Int. J. Refract. Met. Hard Mater. 110 (2023) 106022.
[13] I. Konyashin, F. Schäfer, R. Cooper, B. Ries, J. Mayer, T. Weirich, Novel ultra-coarse hardmetal grades with reinforced binder for mining and construction, Int. J. Refract. Met. Hard Mater. 23 (2005) 225–232.
[14] Q. Cheng, L. Kun, G. Xue-Yi, L. Bin, L. Zheng-Yi, L. Yong, Effect of WC grain size on mechanical properties and microstructures of cemented carbide with medium entropy alloy Co-Ni-Fe binder, J. Cent. South Univ. (Engl. Ed.) 27 (2020) 1146–1157.
[15] T. Soria Biurrun, B. Lopez Ezquerra, L. Lozada Cabezas, J.M. Sánchez Moreno, Effect of milling conditions and binder phase content on liquid phase sintering of heat treatable WC-Ni-Co-Cr-Al-Ti cemented carbides, Int. J. Refract. Met. Hard Mater. 88 (2020) 105202.
[16] X. Wang, Y. Qin, X. Zhu, L. Luo, Y. Wu, Influence of TiB_2 and Ni addition on microstructure and mechanical properties of WC–10Co ultra–coarse grain cemented carbides, J. Alloys Compd. 1039 (2025) 183179.
[17] Milan Grohol, Constanze Veeh, DG GROW, European Commission, Study on the Critical Raw Materials for the EU, Final Report, 2023.
[18] W.D. Schubert, M. Fugger, B. Wittmann, R. Useldinger, Aspects of sintering of cemented carbides with Fe-based binders, Int. J. Refract. Met. Hard Mater. 49 (2015) 110–123.
[19] T. Soria-Biurrun, L. Lozada-Cabezas, F. Ibarreta-Lopez, R. Martinez-Pampliega, J. M. Sanchez-Moreno, Effect of chromium and carbon contents on the sintering of WC-Fe-Ni-Co-Cr multicomponent alloys, Int. J. Refract. Met. Hard Mater. 92 (2020) 105317.
[20] T. Soria-Biurrun, Jose M. Sánchez- Moreno, K. Frisk, Experimental and theoretical study of WC-40Fe-20Co-40Ni, Int. J. Refract. Met. Hard Mater. 102 (2022) 105719.
[21] T. Soria-Biurrun, L. Lozada-Cabezas, J. Navarrete-Cuadrado, F. Ibarreta-Lopez, R. Martinez-Pampliega, J.M. Sanchez-Moreno, Densification of WC-Fe-Ni-Co-Cr cemented carbides processed by HIP after sintering: effect of WC powder particle size, Int. J. Refract. Met. Hard Mater. 110 (2023) 105994.
[22] T. Soria-Biurrun, S. Sridar, K. Frisk, W. Xiong, J.M. Sánchez-Moreno, Experimental investigation and thermodynamic modelling of WC-Fe-Ni-Co-Cr cemented carbides, Int. J. Refract. Met. Hard Mater. 124 (2024) 106824.
[23] N. Hongbo, Z. Qisen, Z. Jianping, W. Xiao, Y. Yang, The preparation, preparation mechanism and properties of extra coarse-grained WC-Co hardmetals, Met. Powder Rep. 72 (3) (2017) 188–194.
[24] F. Aldinger, Controlled porosity by an extreme Kirkendall effect, Acta Metall. 22 (1974) 923–928.
[25] A. Petersson, J. Ågren, Modelling WC-co sintering shrinkage-effect of carbide grain size and cobalt content, Mat. Sci. Eng. A 452-453 (2007) 37–45.
[26] G.S. Upadhyaya, Wetting of ceramics by metal melts- An electronic approach, Sintered Metal-Ceramic Composites, Materials Science Monographs 25, Proc. of the 3rd Int. School on Sintered Materials, New Delhi, Dec 6-9, 1983, pp. 41–50.
[27] M.A. Gren, G. Wahnström, Wetting of surfaces and grain boundaries in cemented carbides and the effect from local chemistry, Mater 8 (2019) 100470.
[28] G.S. Upadhyaya, S.K. Bhaumik, Sintering of submicron WC–10 wt.% Co hard metals containing nickel and iron, Mater. Sci. Eng. A A105–106 (1988) 249–256.
[29] J. Garcia, V. Collado Ciprés, A. Blomqvist, B. Kaplan, Cemented carbide microstructures: a review, Int. J. Refract. Met. Hard Mater. 80 (2019) 40–68.
[30] R. de Oro Calderon, C. Edtmaier, W.-D. Schubert, Novel binders for WC-based cemented carbides with high Cr contents, Int. J. Refract. Met. Hard Mater. 85 (2019) 105063.
[31] I. Borgh, P. Hedström, J. Odqvist, A. Borgenstam, J. Ågren, A. Gholinia, B. Winiarski, P.J. Withers, G.E. Thompson, K. Mingard, M.G. Gee, On the three-dimensional structure of WC grains in cemented carbides, Acta Mater. 61 (2013) 4726–4733.
[32] A. Delanoë, S. Lay, Evolution of the WC grain shape in WC-Co alloys during sintering: effect of C content, Int. J. Refract. Met. Hard Mater. 27 (2009) 140–148.
[33] B.B. Straumal, I. Konyashin, Faceting/roughening of WC/binder interfaces in cemented carbides: a review, Materials 16 (10) (2023) 3696.
[34] Z. Roulon, J.M. Missiaen, S. Lay, Carbide grain growth in cemented carbides sintered with alternative binders, Int. J. Refract. Met. Hard Mater. 86 (2020) 105088.
[35] S. Norgren, J. Garcia, A. Blomqvist, L. Yin, Global trends in the hard metals industry, in: Proceedings 18th Plansee Seminar, Plansee Group, Reutte, 2013 [OS 3/1–29].
[36] J. Gurland, New scientific approaches to development of tool materials, IMR 33 (1988) 151–166.
[37] M. Walbrühl, D. Linder, J. Ågren, A. Borgenstam, A new hardness model for materials design in cemented carbides, Int. J. Refract. Met. Hard Mater. 75 (2018) 94–100.
[38] A. Chychko, J. García, V. Collado Ciprés, E. Holmström, A. Blomqvist, HV-KIC property charts of cemented carbides: a comprehensive data collection, Int. J. Refract. Met. Hard Mater. 103 (2022) 105763.